Preprint of:
Feng-Chuan F. Tsai, Christopher J. O'Brien, Novak S. Petrovic, Aleksandar D. Rakic
"Comparison of Stray-Light and Diffraction-Caused Crosstalk in Free-Space Optical Interconnects"
Proc. SPIE 6038, 388-395 (2006)

Novel Array Geometries for Free-Space Optical Interconnects with Improved Signal-to-Noise Ratio

Feng-Chuan F. Tsai, Christopher J. O'Brien, Novak S. Petrović, Aleksandar D. Rakić
School of Information Technology and Electrical Engineering, The University of Queensland, Brisbane QLD 4072, Australia

ABSTRACT

We investigate the effect of transmitter and receiver array configurations on the stray-light and diffraction-caused crosstalk in free-space optical interconnects. The optical system simulation software (Code V) is used to simulate both the stray-light and diffraction-caused crosstalk. Experimentally measured, spectrally-resolved, near-field images of VCSEL higher order modes were used as extended sources in our simulation model. Our results show that by changing the square lattice geometry to a hexagonal configuration, we obtain the reduction in the stray-light crosstalk of up to 9 dB and an overall signal-to-noise ratio improvement of 3 dB.

Keywords: Stray light crosstalk, free space optical interconnect, diffraction

1. INTRODUCTION

Performance requirements of short-distance digital communication links have increased considerably with the escalating demand for high speed and high density data links. However, large scale electronic systems are suffering from an interconnection bottleneck due to the inductance and capacitance inherent in electric interconnects. The most noticeable limitations are pin congestion, clock skew and bandwidth limitation [1, 2]. The high aggregate bandwidth and channel density achievable by optical interconnects (OIs) make them an ideal replacement for electrical interconnection schemes. Optical interconnects potentially have low power consumption, and can facilitate the development of radically novel designs for VLSI architectures including heterogeneous multiprocessor systems and highly parallel computing systems [3-5]. Recent developments in the integration of Vertical-Cavity Surface-Emitting Laser (VCSEL) arrays and photodetector arrays with CMOS electronic circuitry have increased the practical potential of optical interconnects [6, 7].

Free-space optical interconnects (FSOIs) offer solutions for both chip- and board-level interconnection. Several OI designs based on two dimensional VCSEL arrays have been proposed [8-13]. From these studies, it is evident that one of the major factors that determine the maximum channel density and bit-error ratio is the optical crosstalk noise within the system. The majority of proposed OI designs employ microlenses and other small-diameter optical elements to produce compact optical systems (microchannel architecture). Through the process of miniaturisation, the microlens diameter will decrease to allow for higher channel density; consequently the performance of the system will become increasingly dominated by diffraction.

The generic implementation of a parallel FSOI system consists of two microlens arrays, employed to collimate and focus the laser beams onto an array of photodetectors. The optical power which is correctly transmitted to its intended receiver is the signal, and the portion of the beam which trespasses on neighbouring channels is the crosstalk noise. The two main types of crosstalk mentioned in the literature are the diffraction-caused and stray-light crosstalk noise. Following a number of studies [14-16], diffraction-caused crosstalk noise is modelled as the power incident on unintended receiver microlenses due to diffraction at the transmitter microlenses and the spread of the laser beam between the transmitter microlens array and the receiver microlens array. In our recent paper [17], stray-light crosstalk noise has been referred to as the fraction of the emitter power imaged by the neighbouring transmitter microlens to other channels, possibly far from the intended one. Furthermore, most of the FSOI designs have been based on a simple square geometry.

However, by departing from the square lattice geometry employed by most FSOI architectures, the performance of the FSOI system can be substantially improved [18]. Changing the array geometry into a hexagonal configuration will reduce optical crosstalk noise and improve the signal-to-noise ratio (SNR) of the FSOI system. In addition, VCSELs

tend to operate in several transverse modes simultaneously; the presence of higher order transverse modes will cause a significant degradation in SNR in the OI channel. It is important to account for the effect of higher order transverse modes when designing the FSOI system.

This paper investigates the crosstalk noise in two different geometries of microchannel architecture including the effect of higher order modes. In Sec. 2, the FSOI simulation model is developed. Experimental procedures to obtain the modal content of the VCSEL beam are described in Sec. 3. These experimental findings are used in the simulation model to examine the difference in SLCN and SNR compare two different geometries in Sec. 4. The paper is concluded with a brief discussion in Sec. 5.

2. FSOI SIMULATION MODEL DESCRIPTION

2.1 Design Outline

Figure 1 shows the basic architecture used in the simulations: a microchannel FSOI constructed from two microlens arrays, a VCSEL array, and a photodetector array. The VCSEL array is located at $z = 0$, and the first microlens array is situated at $z = d_1$. The second microlens array is at a distance of $d_2 + d_3$ away from the first microlens array, and the photodetector array is positioned $d_4 = d_1$ away from the second microlens resulting in a symmetrical configuration. The pitch of the system is Δ, and the diameter of the microlens is D. The fill factor, β, is defined as the ratio of the microlens diameter to the array pitch: $\beta = D/\Delta$. Two metrics frequently used to assess interconnect performance are the maximum achievable channel density, $1/\Delta^2$, and the interconnect length, $L = d_1+d_2+d_3+d_4$.

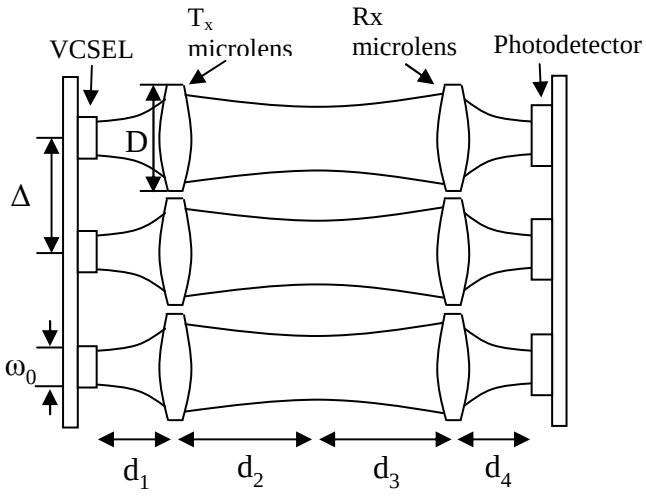

Figure 1: Schematic of a microchannel free-space optical interconnect.

2.2 Design Geometries

We assume the plane of VCSELs, transmitter microlens plane, receiver microlens plane and the plane of the photodetector have the same overall layout. The usual 'square' configuration used in most microchannel architectures is depicted in Fig. 2 (a). We consider the shaded circular aperture as the centre channel of the FSOI system. Another arrangement can be achieved by off-setting each of the outer two rows with respect to the middle reference row [18]. The reference row can be taken to be the one that contains the centre channel. This arrangement is referred to as the 'hexagonal' configuration and it is shown in Fig. 2 (b). Each channel in the square configuration has eight neighbouring channels; channels in the hexagonal arrangement only have six neighbours.

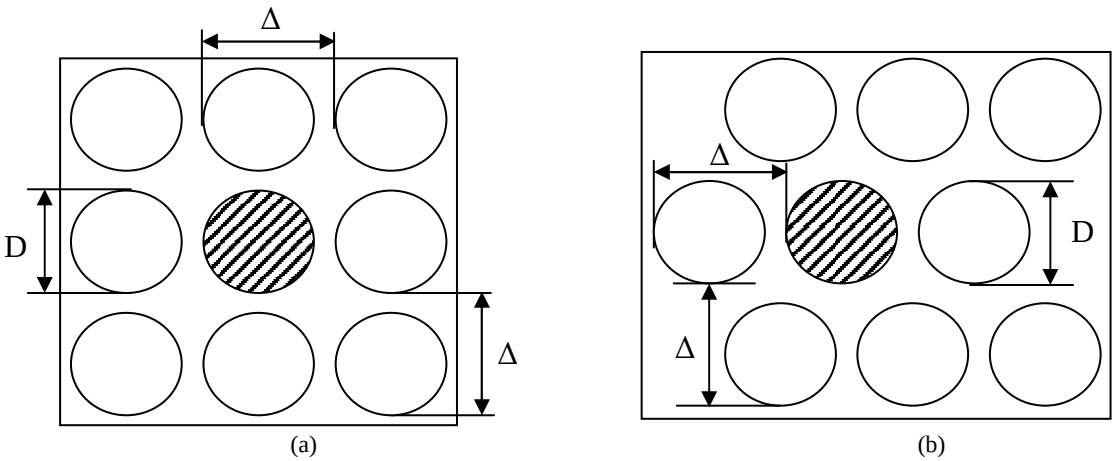

Figure 2: Structure of the T_x or R_x microlens array in (a) normal configuration (b) 'hexagonal' configuration

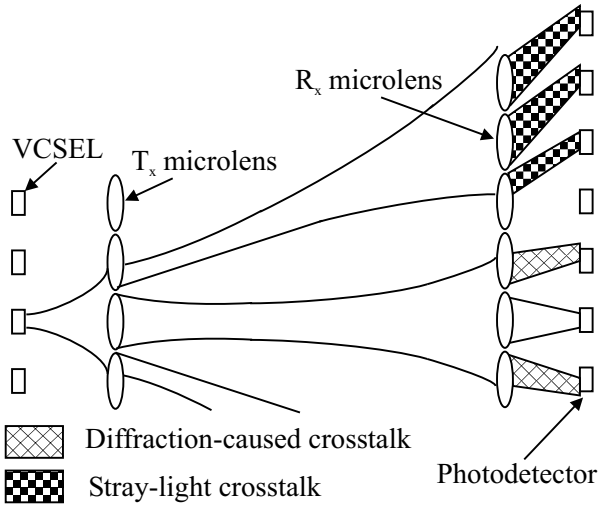

Figure 3: The schematic of free-space optical interconnect showing the diffraction-caused and stray light crosstalk

2.3 Diffraction-caused crosstalk

For each channel, we consider a laser beam of beam waist ω_0, emitted from the transmitter plane through its corresponding transmitter microlens and imaged to the intermediate beam waist. The beam propagates from the intermediate beam waist to the intended receiver microlens. Due to the diffraction-caused spreading of laser beams, the beam radius at the receiver microlens frequently exceeds the radius of the receiver microlens. Therefore, a fraction of the transmitted power will fall on the microlenses adjacent to the intended microlens, and will be focussed onto unintended photodetectors, Fig. 3, introducing crosstalk noise. This noise is usually assumed to be the dominant component of the optical crosstalk noise. In this article we will refer to it as the diffraction-caused crosstalk noise (DCCN). Therefore, the DCCN is defined as the optical power that propagates through the intended transmitter microlens, but falls onto an adjacent receiver microlens and is focussed onto photodetectors for which it was not intended.

2.4 Stray-light crosstalk

We now consider another source of optical crosstalk, introduced by [17]. Again, we consider an arbitrary channel within the microchannel architecture, depicted by Fig 3. In this case, we concentrate on the fraction of power emitted by the VCSEL that falls on the transmitter microlenses adjacent to the intended transmitter lens. Due to the curvature of the microlenses, the beam is refracted away from the intended channel as shown in Fig 3. As it propagates through the system, the beam will further expand until it reaches the receiver microlens plane. Unlike the diffraction-caused crosstalk, where most of the noise can be attributed to the adjacent channels, the beam can be redirected to photodetectors far from the intended channel. Therefore, in our simulations we depart form the usual analysis in which a

channel will only contribute noise to its nearest neighbours. In this study we demonstrate that, once stray-light crosstalk is properly accounted for, significant crosstalk can be introduced to a receiver by non-neighbouring channels. This type of crosstalk, caused by the overfill of the transmitter microlens, will be referred to as stray-light crosstalk noise (SLCN) throughout this article.

To calculate the crosstalk noise present in the central channel, we consider the noise induced on a central photodetector by all the channels surrounding it. However, the same result can be obtained by calculating the optical power falling on the surrounding photodetectors from the central channel. In this manner, the computational complexity of calculating the signal and noise powers can be greatly reduced by considering the transmission of a single beam over a large area, instead of the propagation of a large number of beams into a localised area.

3. EXPERIMENTAL MEASUREMENT OF HIGHER ORDER TRANSVERSE MODES

For drive currents above threshold, VCSELs typically operate simultaneously in several higher-order transverse modes. In addition to lasing at a slightly different wavelength, these transverse modes propagate with a larger spot size than the fundamental mode and diverge more quickly. The modal composition of a VCSEL is, therefore, an important consideration when attempting to calculate the crosstalk noise in an optical interconnect.

The beam profiles of the transverse modes can be described by two families of orthogonal solutions to the paraxial wave equation: the Hermite-Gaussian (HG) and Laguerre-Gaussian (LG) modes. The LG profiles, expressed in cylindrical coordinates, are the most appropriate representation for our purposes and are presented below [19]:

$$\begin{Bmatrix} \psi_{nm}(r,\theta,z) \\ \psi_{nm}^{*}(r,\theta,z) \end{Bmatrix} = K_{nm}\left(\frac{r\sqrt{2}}{w(z)}\right)^{m} L_n^{(m)}\left(\frac{2r^2}{w(z)^2}\right)\exp\left(\frac{-r^2}{w(z)^2} - j\frac{kr^2}{2R(z)}\right)\begin{Bmatrix} \cos(m\theta) \\ \sin(m\theta) \end{Bmatrix} \tag{1}$$

where,

$$K_{nm} = A_{nm}N_{nm} \tag{2}$$

and,

$$A_{nm} = \exp\left\{ j\left[(2n+m+1)\arctan\frac{\lambda(z-z_s)}{\pi w_s^{\,2}} - k(z-z_s) \right] \right\} \tag{3}$$

and,

$$N_{nm} = \frac{2}{w(z)\sqrt{\pi(1+\delta_{om})}}\left[\frac{n!}{(n+m)!}\right]^{1/2} \tag{4}$$

In the above equations, the wave number is $k = 2\pi/\lambda$, and the Rayleigh range is given as $z_R = \frac{1}{2}k\, w_s^{\,2}$, where w_s is the beam waist and is located at $z = z_s = 0$. The beam radius at any distance along the propagation axis is given as:

$$w(z) = w_s\sqrt{1+\left(\frac{z}{z_R}\right)^2} \quad , \tag{5}$$

and the radius of curvature is

$$R(z) = z\left[1+\left(\frac{z_R}{z}\right)^2\right] \quad . \tag{6}$$

Equation (3) shows the Guoy phase shift experienced by the laser beams. Higher-order modes (n, $m > 0$) will experience a greater phase shift than the fundamental Gaussian mode, and will resonate at shorter wavelengths inside a cavity. This explains the spectral separation of transverse modes in a laser.

In order to examine the effect of transverse modes, it is necessary to determine the modal content of practical devices. Experiments were performed on a commercially available VCSEL (*Mode 8085-2008*). The continuous-wave, room temperature optical spectra were measured at drive currents up to $7\times I_{th}$, at intervals of 0.05 mA. From this data, the evolution of the VCSEL spectrum was examined and a modally resolved light-current curve was constructed.

From the spectra, the presence and relative power of higher order modes can be observed, but their spatial profiles can not be identified. To accomplish this, an actuator controlled fibre probe was used to scan a cross section of the magnified near field of the laser beam. At each point of a 15×15 grid, the spectrum was recorded, and the modal peaks were isolated. From these measurements we determined the optical power associated with each individual mode at each spatial pixel. The dominant lasing modes of this VCSEL can be identified as: LG_{00}, LG_{01}, LG_{02}, and an $LG_{10} + LG_{02}$ combination, shown in Fig. 4.

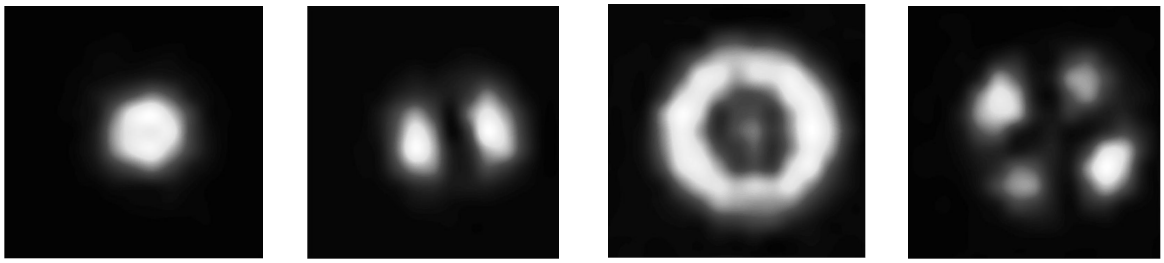

LG_{00} LG_{01} $LG_{10} + LG_{02}$ LG_{02}

Figure 4. Mode patterns of Laguerre-Gaussian modes

4. SIMULATION RESULTS

Commercial simulation software, Code V, is used to simulate both the SLCN and DCCN. The design parameters used for simulation are as follows: the pitch between the channels is 250 μm, the beam has a waist radius of 3 μm and a central wavelength of 850 nm. The transmitter and receiver microlenses are assumed to be spherical lenses, made from BK7 optical glass, with a 95% fill factor. The focal length of all microlenses is 800 μm and the distance between the VCSEL and the transmitter microlens is fixed at $d_1 = f + z_R$, where f is the microlens focal length, and z_R is the Rayleigh range. The simulation was performed on a two-dimensional, lattice microlens array of 64×64 channels. Both the SLCN and DCCN are measured by the optical power incident upon unintended receiver microlenses. The SNR is defined as follows

$$SNR = 10\log_{10}\frac{S}{SLCN + DCCN} \tag{7}$$

where S is the normalized optical power received by the corresponding photodetector.

Optical interconnect designs are typically evaluated by considering the propagation of point sources or from the uniform surface emitters. To determine the effect of higher order transverse modes on FSOI performance, we propagate a two-dimensional beam profile through the optical system. The extended sources used in these simulation experiments are based on the experimentally determined modal structure of the VCSEL beams measured in Sec. 3. and are formed by the weighted combination of the following Laguerre-Gaussian modes: LG_{00}, LG_{01}, LG_{10}, and LG_{20}. The mode patterns used in the simulation are shown in Fig 4. For each mode, the calculated transverse profile is mapped onto a 101×101 point computational grid used as the beam definition for the diffraction-based beam propagation. A combination of geometrical ray tracing and diffraction-based propagation techniques are used to trace the beam through the optical interconnect.

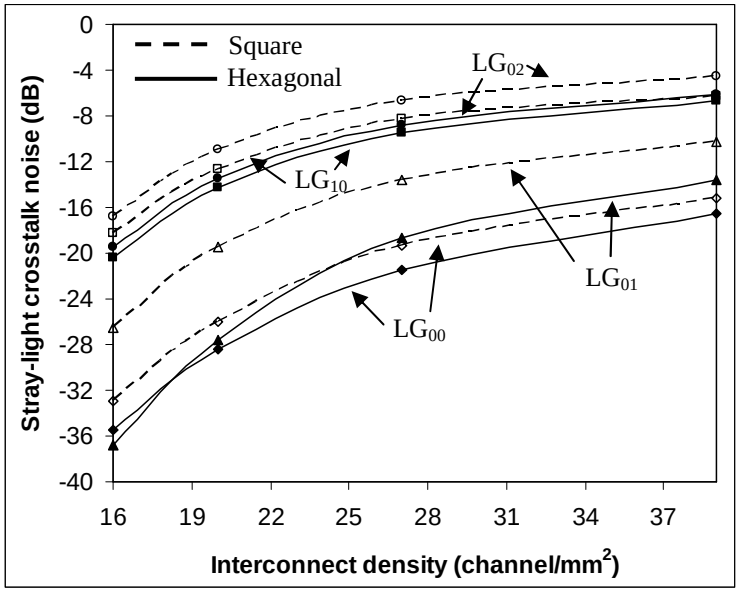

Figure 5. Stray-light crosstalk noise is normalised to the power of the emitted beam and then calculated using a log scale: Normalised Stray-light crosstalk noise with increasing system capacity (channels per mm^2) for different modes.

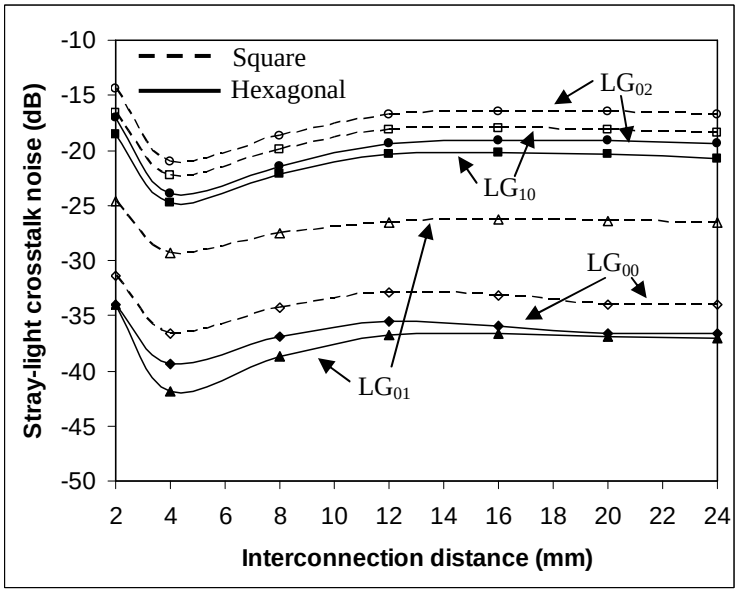

Figure 6. Stray-light crosstalk noise is normalised to the power of the emitted beam and then calculated using a log scale: Normalised Stray-light crosstalk noise with increasing interconnection distance for different modes.

Figure 5 shows the comparison between square and hexagonal configuration for SLCN with different transverse modes and increasing channel density. For both configurations, the SLCN increases with channel density, and interconnect performance degrades further with the presence of higher order modes. Comparing the configurations, it can be said that hexagonal design reduces the SLCN by around 3 dB, 9 dB, 2 dB and 3 dB for LG_{00}, LG_{10}, LG_{10}, and LG_{02} respectively. The variations of reduction in SLCN value are dependant on the geometrical properties of the incident beam. In Fig. 6 the SLCN for the square and hexagonal configuration with different transverse modes and increasing interconnect distance is compared. As before, the hexagonal configuration exhibits less SLCN for all transverse modes considered. Since SLCN is mostly independent of interconnection distance, performance improvement is constant with increasing distance.

Figure 7 shows SNR for both square and hexagonal configuration with different transverse modes and increasing channel density. The interconnection distance of 12 mm was maintained as the interconnect density was increased, and several transverse modes were propagated through the interconnect. It is evident that the hexagonal arrangement provides the better performance than the square geometry. The interconnect SNR increased by apparently 3 dB for all transverse modes, when the hexagonal configuration is implemented.

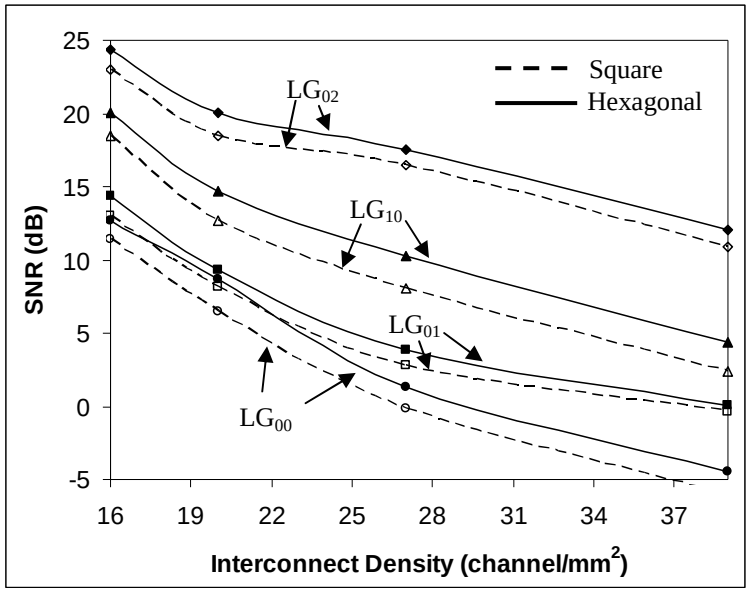

Figure 7. Signal-to-noise ratio with increasing system capacity (channels per mm^2) for different modes.

5. CONCLUSION

The characteristic of the SLCN using hexagonal arrangement has been investigated for the first time to our knowledge. The numerical simulation has been performed using a combination of exact ray tracing and the beam propagation methods. The SLCN and SNR using hexagonal configuration have been compared with that of the square geometry. In all cases considered, the implementation of a hexagonal design reduced the SLCN and increased the SNR. The level of improvement is dependent on the optical structure of the incident beam, but SNR increase of up to 3 dB was observed.

REFERENCES

1. D. A. B. Miller, "Invited paper: Physical reasons for optical interconnection," International Journal of Optoelectronics Vol. 11, pp. 155-168, 1997.
2. D. A. B. Miller, “Rationale and challenges for optical interconnects to electronic chips,” Proceedings of IEEE, Vol. 88, pp. 728-749, 2000.
3. D. V. Plant and A. G. Kirk, "Optical interconnects at the chip and board level: challenges and solutions," Proceedings of IEEE, Vol. 88, pp. 806-818, 2000.
4. D. Fey, W. Erhard, M. Gruber, J. Jahns, H. Bartelt, G. Grimm, L. Hoppe, and S. Sinzinger, "Optical interconnects for neural and reconfigurable VLSI architecture," Proceedings of IEEE, Vol. 88, pp. 838-847, 2000.
5. N. McArdle, M. Naruse, H. Toyoda, Y. Kobayashi, and M. Ishikawa, "Reconfigurable Optical Interconnections for Parallel Computing," Proceedings of IEEE, Vol. 88, pp. 829-837, 2000.
6. K. M. Geib, K. D. Choquette, D. K. Serkland, A. A. Allerman, and T. W. Hargett, "Fabrication and performance of two-dimensional matrix addressable arrays of integrated vertical-cavity lasers and resonants cavity photodetectors," IEEE Journal of Selected Topics in Quantum Electronics, Vol. 8, pp. 943-947, 2002.
7. R. H. Havemann and J. A. Hutchby, "High-Performance Interconnects: An Integration Overview," Proceedings of IEEE, Vol. 89, pp. 586-601, 2001.

8. M. Châteauneuf, A. G. Kirk, D. V. Plant, T. Yamamoto, and J. D. Ahearn, "512-channel vertical-cavity surface-emitting laser based free-space optical link," Applied Optics, Vol. 41, pp. 5552-5561, 2002.
9. M. W. Haney, M. P. Christensen, P. Milojkovic, J. Ekman, P. Chandramani, R. Rozier, F. Kiamilev, Y. Liu, and M. Hibbs-Brenner, "Multichip free-space global optical interconnection demonstration with integrated arrays of vertical-cavity surface-emitting lasers and photodetectors," Applied Optics, Vol. 38, pp. 6190-6200, 1999.
10. E. M. Strzelecka, D. A. Louderback, B. J. Thibeault, G. B. Thompson, K. Bertilsson, and L. A. Coldren, "Parallel free-space optical interconect based on arrays of vertical-cavity lasers and detectors with monolithic microlenses," Applied Optics, Vol. 37, pp. 2811-2821, 1998.
11. R. Wong, A. D. Rakic, and M. L. Majewski, "Design of microchannel free-space optical interconnects based on vertical-cavity surface-emitting laser arrays," Applied Optics, Vol. 41, pp. 3469-3478, 2002.
12. R. Wong, A. D. Rakic, and M. L. Majewski, "Analysis of lensless free-space optical interconnects based on multi-transverse mode vertical-cavity-surface-emitting lasers," Optics Communications, Vol. 167, pp. 261-271, 1999.
13. X. Zheng, P. J. Marchand, D. Huang, and S. C. Esener, "Free-space parallel multichip interconnection system," Applied Optics, Vol. 39, pp. 3516-3524, 2000.
14. N. S. Petrovic and A. D. Rakic, "Modeling diffraction in free-space optical interconnects by the mode expansion method," Applied Optics, Vol. 42, pp. 5308-5318, 2003.
15. X. Zheng, P. J. Marchand, D. Huang, O. Kibar, and S. C. Esener, "Cross talk and ghost talk in a microbeam free-space optical interconnect system with vertical-cavity surface-emitting lasers, microlens, and metal-semiconductor-metal detectors," Applied Optics, Vol. 39, pp. 4834-4841, 2000.
16. F. Lacroix, M. Châteauneuf, X. Xue, and A. G. Kirk, "Experimental and numerical analyses of misalignment tolerances in free-space optical interconnects," Applied Optics, Vol. 39, pp. 704-713, 2000.
17. F. F. Tsai, C. J. O'Brien, N. S. Petrovic, and A. D. Rakic, "Analysis of optical channel cross talk for free-space optical interconnects in the presence of higher-order transverse modes," Applied Optics, Vol. 44, pp. 6380-6387, 2005
18. N.S. Petrvoic, A.D. Rakic, and M. L. Majewski, "Free-space optical interconnect with improved signal-to-noise ratio," in Proceedings 27th European Conference on Optical Communication ECOC 2001, Vol .3 pp 292-3, 2001
19. A. E. Siegman, *Lasers*, University Science Books, Sausalito, Cal, 1986.